Anomalous inter-membrane cholesterol transport in fluid phase phosphoserine vesicles driven by headgroup ordered to disordered entropic transition

Sumit Garg[a,1], Yangmingyue Liu[a,1], Ursula Perez-Salas[a,1,*], Lionel Porcar[b,2], Paul D Butler[c,2]

[a] *Physics Department, University of Illinois at Chicago, Chicago, IL 60607, USA*
[b] *Institut Laue Langevin, 71 Avenue des Martyrs, 38042 Grenoble Cedex 9, France*
[c] *NIST Center for Neutron Research, National Institute of Standards and Technology, Gaithersburg, MD 20899-6102, USA*

A B S T R A C T

POPS is highly enriched in the inner leaflet of the plasma membrane. Here we present measurements of inter-membrane cholesterol transport rates in POPS vesicles. We find that the cholesterol transport kinetics are not only an order of magnitude slower than in POPC lipids at near physiological temperatures, they exhibit a surprising discontinuous Arrhenius behavior around 48 °C. Moreover, thermodynamic analysis suggests that for biologically relevant temperatures, below the discontinuity, the exchange of cholesterol is entropically dominated while it is enthalpically driven, as is the case in POPC vesicles, above that discontinuity. Using the polar fluorescent probe Laurdan we found that POPS *fluid* membranes retain a large degree of order in the headgroup region for temperatures below the discontinuity but undergo an order-to-disorder transition in the region coinciding with the discontinuity in the transport of cholesterol in POPS membranes providing an explanation not only for the discontinuity but for the entropic dominance at physiological temperatures.

1. Introduction

Cholesterol is an essential structural component of most mammalian cells, with proper cholesterol levels being vital to a host of cellular functions such as signal transduction, membrane fluidity and rigidity, protein interactions, and membrane trafficking that, if deficient, lead to disease (Ikonen, 2008; van Meer et al., 2008; Maxfield and Tabas, 2005). Intracellular cholesterol transfer is critical for cellular cholesterol homeostasis, maintaining an uneven distribution throughout the membranes of the cell; for example, 60–70% of cellular cholesterol is present in the plasma membrane and only 0.01–0.5% is found in the endoplasmic reticulum, where it is synthesized (Soccio and Breslow, 2004). One mechanism thought to be contributing to such a distribution gradient is the difference in affinity of cholesterol for various lipids (van Meer et al., 2008).

This idea has led to numerous studies to investigate and characterize cholesterol-lipid interactions. Most of these studies have focused on saturated lipids, which interact with cholesterol to form lipid domains known as lipid rafts (Simons and Ikonen, 1997; Lingwood and Simons, 2010). Thus relatively little attention has been given to unsaturated lipids which appear to have less favorable interactions with cholesterol (Frazier et al., 2007). Interestingly, the interactions may be so unfavorable, as in the case of polyunsaturated lipids, that they may

also play an important role in lipid raft formation (Wang et al., 2017; Kucerka et al., 2010).

The use of model systems makes it possible to directly probe cholesterol-lipid interactions (Eeman and Deleu, 2010; Simons and Vaz, 2004). However, even in these simplified systems interpreting how lipids and cholesterol interact can be unclear. For example, it has been reported that it is more difficult for cyclodextrin to eject cholesterol from POPS membranes than from POPC membranes, which suggests a higher affinity of cholesterol to POPS (Leventis and Silvius, 2001; Niu and Litman, 2002). On the other hand, nuclear magnetic resonance (NMR), X-ray diffraction, calorimetry and electron paramagnetic resonance (EPR) have reported the detection of bilayer cholesterol crystal structures within POPS membranes starting at a relatively low concentration of cholesterol (in the vicinity of 35 mol%) (Epand et al., 2002; Raguz et al., 2011) which suggests a low affinity for POPS (Epand et al., 2002) and also explains why it is difficult to eject cholesterol from POPS with cyclodextrin. However we have shown that in small (100 nm diameter) unilamellar vesicles cholesterol saturates both POPC and POPS membranes to high molar fractions, 61 mol% and 73 mol% respectively (Garg et al., 2014) and found no evidence of cholesterol-only domains within POPS membranes (Krzyzanowski et al., 2015). This experimental result was also supported by coarse-grained molecular dynamics simulations (Garg et al., 2014) which, together, suggest
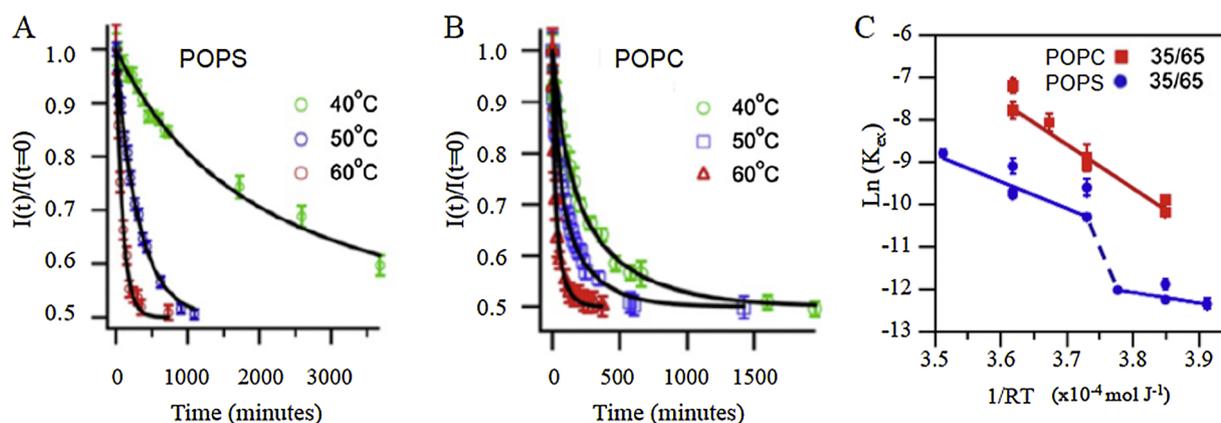
Fig 1. Comparison of normalized intensity decay curves for cholesterol transport between 100 nm lipid vesicles made of POPS (A) and POPC (B) at three different temperatures. (C) Arrhenius plots for the rate of inter-membrane exchange in POPC and POPS. Transfer rates were measured such that the donor population had an initial 35% mole fraction of cholesterol. The rates are reported in s^{-1}. Error bars represent a 1 sigma uncertainty level.

a slightly higher affinity of cholesterol for POPS than POPC.

2. Results and discussion

Here we take a different approach to investigating the interaction of cholesterol with POPS. Using time resolved small angle neutron scattering (TR-SANS) we were able to follow the exchange of cholesterol between unilamellar POPS vesicles. The protocol, described in detail elsewhere (Garg et al., 2011), consists of mixing cholesterol-containing donor vesicles (containing 35% mole fraction of cholesterol, a concentration relevant to biological membranes (van Meer et al., 2008)) and cholesterol-free acceptor vesicles in equal amounts. The SANS intensity is recorded as a function of time while cholesterol transfers and equilibrates between vesicles. The solvent and lipid deuteration level are carefully chosen so as to render the lipids completely invisible. The scattered intensity is thus exclusively due to cholesterol and decreases as a result of the transfer process between donor and acceptor vesicles. Because the shape and size of the donor and acceptor vesicles remain the same throughout the exchange process, the scattered intensity ultimately reaches half its initial value when equilibrium is reached (Garg et al., 2011). Fig. 1A and B show the normalized intensity decay curves for cholesterol transfer in 100 nm POPS and POPC vesicles at 3 different temperatures. As expected, the equilibrium value of 0.5 is reached faster at higher temperatures. Indeed, an equilibrium value of 0.5 in the normalized intensity decay curves guarantees that we do not lose vesicles to fusion events, which for POPS vesicles is not surprising given there is charge repulsion. Kinetic rate constants (inter-membrane exchange, k_{ex}, and intra-membrane transfer or flip-flop, k_f) are extracted from fits to these decay curves using the two-process model (exchange and flip-flop) used previously for the POPC system (Garg et al., 2011). The transfer of cholesterol between POPS vesicles, however, was such that the intensity decay was only sensitive to the exchange of cholesterol. Indeed, flipping is detected if it is rate limiting to the exchange process (Garg et al., 2012). Thus it appears that in contrast to the POPC/cholesterol system, in POPS/cholesterol the exchange of cholesterol between vesicles is significantly slower than the flipping rate of cholesterol making the latter inaccessible in these experiments. Fig. 1C shows the Arrhenius plot for the exchange process. This plot highlights the significantly slower cholesterol exchange rates in POPS vesicles compared to those in POPC vesicles. Most surprising however is the precipitous drop in exchange rates occurring between 46 °C and 50 °C for the POPS system. Such a discontinuity requires a significant change in the energetics of the activation process and is reminiscent of the first order-like transition occurring in the case of cholesterol or lipid transport in vesicles when crossing the lipid melting temperature, T_m (Kleinfeld and Storch, 1993; Masserini and Freire, 1987; Gerelli et al.,

2013). To the best of our knowledge such anomalous cholesterol transport behavior in lipid membranes in the *fluid phase* has never been reported.

Treating each temperature regime as a separate exchange process, thermodynamic parameters for each state can be extracted using Eyring's transition state theory (Eyring, 1935; Laidler and Klng, 1983) as implemented by Homan and Pownall (Homan and Pownall, 1988), and given by Eq. (1). The enthalpy is related to the activation energy, E_a by: $\Delta H^\dagger = E_a - RT$, where E_a corresponds to the slope of the linear fit for the rates in the Arrhenius plot (Fig. 1C) and the † represents transition state quantities. The difference between the enthalpy, $\Delta H^\dagger$, and entropy, $T\Delta S^\dagger$, terms is the free energy: $\Delta G^\dagger = \Delta H^\dagger - T\Delta S^\dagger$. The corresponding thermodynamic parameters obtained from the E_a's are reported in Table 1.

$$e^{\Delta S^\dagger/R} = \frac{N_A h}{RT} K_{T^*} e^{\Delta H^\dagger/RT}$$

(1)

where N_A, h, R are Avogadro's number, Plank's constant and the gas constant respectively. T is temperature in Kelvin and K_{T^*} corresponds to the exchange rates extrapolated to 37 °C (310 K).

The results reported in Table 1 suggest that the energetic barrier that cholesterol has to overcome to exchange, while essentially enthalpic in POPC membranes, has a significant entropic component in POPS membranes. In particular we find that entropy completely dominates at the lower, most biologically relevant temperatures. Interestingly we find that in POPS, the relative importance of the enthalpic and entropic contributions to cholesterol exchange are reversed upon crossing the discontinuity in the Arrhenius plot.

The lack of an endothermic signature or a structural change (Krzyzanowski et al., 2015), along with the entropic nature of the barrier to exchange in POPS, suggested a transition of a different kind. To detect possible subtle changes in the state of the membrane which could be responsible for such a behavior, we used the fluorescent polarized molecular probes Laurdan and DPH which partition preferentially into membranes in aqueous environments (Demchenko et al., 2009). Laurdan's emission spectra varies according to

Table 1
Thermodynamic parameters extracted from E_a values obtained from the fits to the temperature dependent exchange rates shown in Fig. 1C for cholesterol transport in POPC and POPS model membranes with an initial cholesterol concentration of 35% mole fraction in donor vesicles.

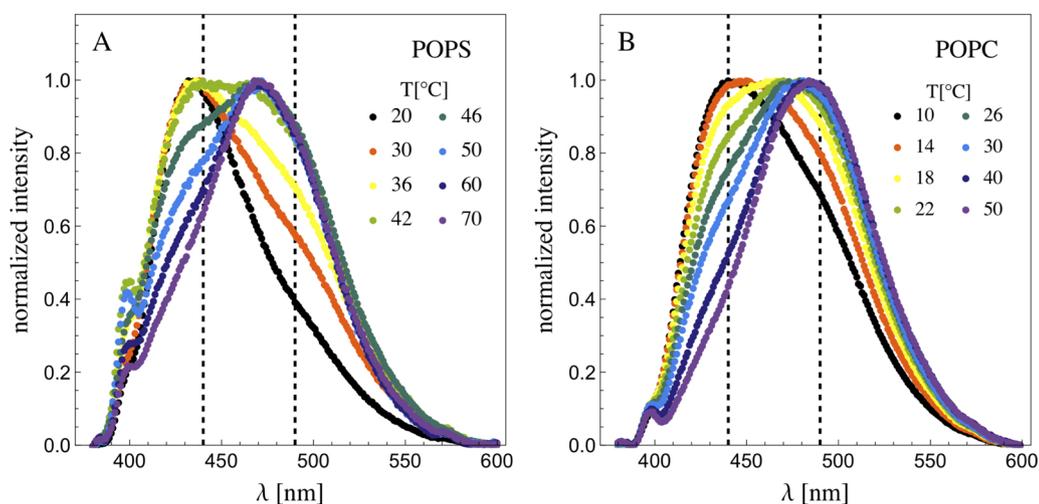|	$t_{1/2}$ (min)	$\Delta H^\dagger$ (kJ/mol)	$T\Delta S^\dagger$ (kJ/mol)	$\Delta G^\dagger$ (kJ/mol)
POPS 50 °C	423 ± 10	61 ± 5	49 ± 5	109 ± 10
POPS 46 °C	2030 ± 37	23 ± 5	88 ± 5	111 ± 10
POPC 50 °C	88 ± 2	101 ± 5	7 ± 5	107 ± 10

Fig. 2. Laurdan emission spectra (excitation wavelength, 340 nm) of (A) POPS, (B) POPC for a range of temperatures where the initial low temperature peak is seen to experience a red-shift as temperature increases. The temperature at which the intensity at 490 nm becomes greater than at 440 nm, corresponds to the order to disorder transition.
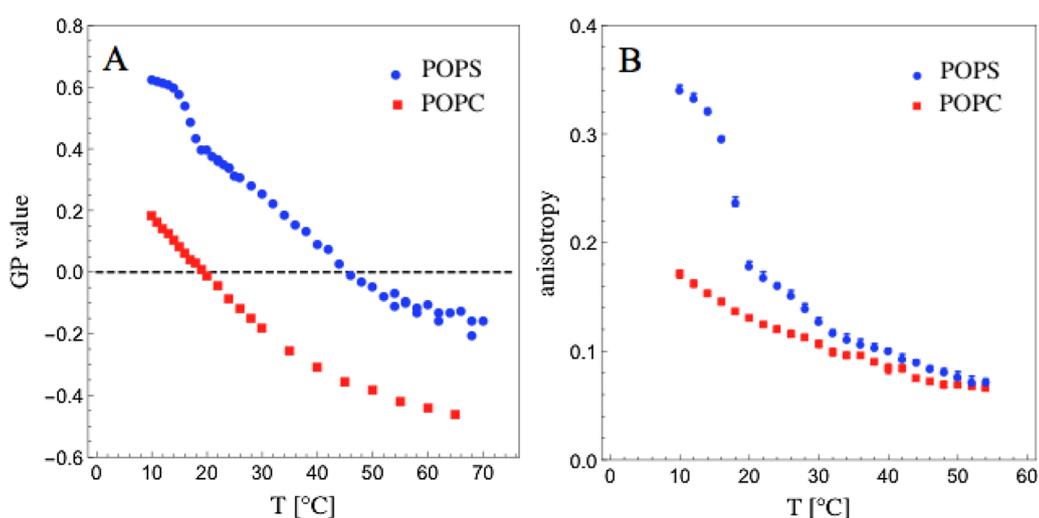

Fig. 3. (A) *GP* values obtained using Laurdan for POPS (blue circles) and POPC (red squares) as a function of *T* (°C). The plateau in the *GP* value at low temperature for POPS corresponds to the gel phase. A transition from a positive to negative *GP* value is indicative of Laurdan becoming highly exposed to water in the headgroup, thus suggesting an order to disorder transition in this region. (B) Corresponding steady-state anisotropy DPH data (Troup et al., 2006) for POPS and POPC. An abrupt reduction in anisotropy occurs in the tail region of POPS as expected during melting (at 14 °C) (Lakowicz and Prendergast, 1978). After this transition, POPS shows a slow but steady decrease in anisotropy with increasing temperature expected for a tail in the liquid disordered state (Lakowicz and Prendergast, 1978). POPC also shows this steady decrease in anisotropy, with the two systems becoming comparable above 50 °C. The error bars correspond to five measurements per point. (For interpretation of the references to color in this figure legend, the reader is referred to the web version of this article.)

dipole–dipole interactions with the surrounding environment and is therefore particularly sensitive to water accessibility to the headgroup region of the membrane (Parasassi et al., 1990; Harris et al., 2002). On the other hand, DPH partitions into the tail region of the membrane and is sensitive to local chain order (Lenz, 1989). Fig. 2 shows the emission spectra of Laurdan in POPS and in POPC. The spectra is characterized by a peak centered at 440 nm that red shifts as the temperature increases. This red shift is due to changes in water accessibility in the headgroup region. The generalized polarization function, *GP*, given by Eq. (2), quantifies this effect by comparing the relative differences in intensity of the spectra at two wavelengths, 440 nm and 490 nm, shown as dashed lines in Fig. 2 (Jay and Hamilton, 2017). In Fig. 3A the *GP* values for POPS and POPC are plotted as a function of temperature. In POPS we see the characteristic positive plateau in the *GP* values of the gel state below 14 °C. At this temperature, the T_m of POPS, there is a sharp drop in the *GP* value, but in contrast to the behavior observed in saturated lipids where the gel to fluid transition is accompanied by a precipitous drop from positive (between 0.6 and 0.8) to negative *GP* values in a narrow temperature range (Parasassi et al., 1990, 1991; Harris et al., 2002), the *GP* value remains positive. As temperature increases further, the *GP* value steadily decreases and, at about 30 degrees above T_m, the *GP* value becomes negative. In POPC we also observe a transition from a positive to a negative *GP* value occurring in the vicinity of $T = 20$ °C, which is about 22 degrees higher than its T_m. A *GP*

value of zero marks the transition from a mostly *ordered* state, where water barely penetrates the headgroup to a mostly *disordered* state in which the headgroup has significant exposure to bulk water.

Using DPH's steady-state anisotropy response to polarized light, quantified through Eq. (3), it is possible to assess the fluidity of the tail region of the membrane. As shown in Fig. 3B we find no change in the tail order in either POPS or POPC when the *GP* value becomes zero. The remarkable coincidence of cholesterol transitioning from nearly immobile to mobile in POPS between 46 °C and 50 °C and POPS' headgroup reaching a predominantly *disordered* state suggests that the discontinuous transition of cholesterol transfer in POPS may in fact be driven by this order-to-disorder transition in the headgroup rather than any fluidity or ordering effects of cholesterol on the membrane. Because POPC also displays a headgroup transition from mostly *ordered* (with positive GP values) to mostly *disordered* (with negative GP values), there should be a similar discontinuity in cholesterol's exchange in POPC. However, as shown in Fig. 4, the predicted exchange rates in the vicinity of $T_{GP=0}$ would make it difficult to probe on experimentally accessible timescales.

3. Conclusion

We found that the rate of cholesterol transport is roughly five to ten times slower in POPS than in POPC. However, while the intervesicular
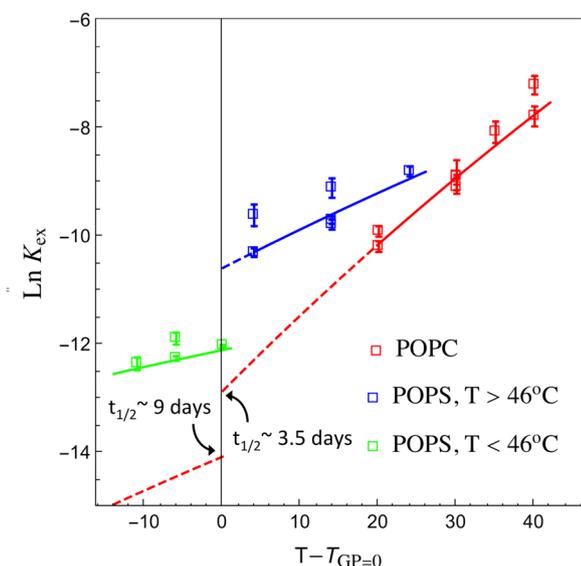
Fig. 4. Rates of cholesterol in POPC and POPS (donor vesicles with 35 mol% cholesterol) vs $T - T_{GP=0}$. $T_{GP=0}$ corresponds to the temperature at which the *GP* value changes from positive to negative upon increasing the temperature. The dashed lines extrapolate to the rates at which a discontinuous exchange rate is expected in POPC as well as the anticipated discontinuous drop in the rates. These rates are, from this extrapolation, expected to be slower than for POPS, particularly for temperatures below $T_{GP=0}$, which make it difficult to probe given the life-time of vesicles and lipids as well as the experimentally accessible timescales at neutron scattering facilities.

cholesterol kinetics in POPC follows a normal Arrhenius behavior in the temperature range probed, the transfer process in POPS exhibits a surprising discontinuity between 46 °C and 50 °C. This transition seems independent of the initial cholesterol concentration in the vesicles as shown in Fig. 5A. Above this transition, however, the exchange of cholesterol behaves enthalpically, as is the case of POPC, and the differences in the exchange rates of cholesterol between POPC and POPS can be explained by the difference in their T_m (Fig. 5B). On the other hand, at temperatures below 46 °C, cholesterol exchange in POPS is nearly frozen and entropically dominated. Using Laurdan and DPH, we discovered that in these unsaturated lipids, POPC and POPS, there appears to be an order-to-disorder transition occurring in the headgroup region well above the order-to-disorder transition temperature of the

tail region that signals the gel to fluid transition, T_m. Indeed, the tail region remains fluid throughout this transition (Fig. 3B). Remarkably, this head group order–disorder transition in POPS occurs at the same temperature as its anomalous Arrhenius behavior, consistent with the entropic transition suggested by the thermodynamic analysis of the TR-SANS data and suggesting this may be a more general phenomenon. In closing, it is interesting that at biologically relevant temperatures (below the anomalous transition), cholesterol is nearly frozen in POPS membranes. Given the presence of POPS in the inner leaflet of the plasma membrane (van Meer et al., 2008), this could certainly contribute to enhanced entrapment of cholesterol in the plasma membrane, even without saturated lipids.

4. Materials and methods

4.1. Materials

A fully deuterated palmitoylated tail in 1-palmitoyl-2-oleoyl-phosphatidyl-serine (POPS) and 1-palmitoyl-2-oleoyl-phosphatidylcholine (POPC) was obtained from Avanti Polar Lipids (Alabaster, AL). Deionized water was purified with a Millipore Simplicity UV purifier and was used for all solutions. D_2O was obtained from Cambridge Isotope Laboratories, Inc.

The lipids, in powder form, were used as received. When making vesicles with cholesterol precise amounts of POPS or POPC and cholesterol were weighed out in glass vials. Chloroform was added to the vials and stirred sufficiently to dissolve all lipids. Dry lipid films were obtained by applying a constant stream of nitrogen to the chloroform solutions in the vials. The vials were then placed in a vacuum oven overnight at 60 °C to assure the complete removal of chloroform. The dried POPS/cholesterol or POPC/cholesterol lipid films were then dispersed in aqueous solutions made exclusively with D_2O and H_2O at appropriate ratios to achieve the correct neutron contrast match point for POPS or POPC. For vesicles devoid of cholesterol, POPS or POPC powder was directly dispersed in the same D_2O and H_2O mixture as the vesicles with cholesterol. 100 nm diameter unilamellar vesicles were formed via the extrusion method using a mini-extruder from Avanti Polar Lipids with 1 mL Hamilton syringes and 100 nm polycarbonate membranes. A relatively low polydispersity solution of 100 nm small unilamellar vesicles (SUVs) was achieved by flowing the aqueous lipid solutions through the membrane 41 times at 40 °C. This temperature is well above the melting temperature of POPS.

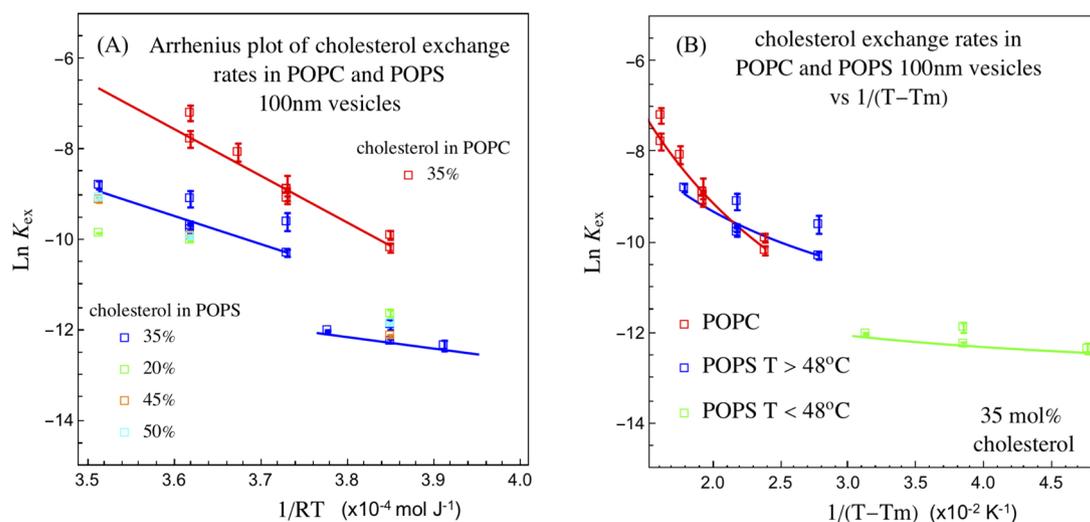Fluorescent probe Laurdan (6-dodecanoyl-2-

Fig. 5. (A) Arrhenius plots for initial fractions of cholesterol in POPS: 20%, 25%, 35%, 45% and 50%, including POPC with 35% cholesterol for comparison. The continuous lines correspond to weighted linear fits to the 35% cholesterol data. (B) Rates vs $1/(T - Tm)$ in POPC and POPS with 35 mol% cholesterol. The high temperature data for POPS roughly overlaps with the POPC data.

dimethylaminonaphthalene) was purchased from Molecular Probes while DPH (1,6-diphenyl-1,3,5-hexatriene) was obtained from Sigma Aldrich. 3 μL Laurdan in methanol stock solution (0.12 mM) is added to lipid vesicles so that the lipids to Laurdan molar ratio is 1000:1. DPH is incorporated into lipid vesicles by mixing them in choloroform with lipids to a ratio of 1000:1 as well. The mixture is then dried in vacuum at 60 °C overnight.

4.2. Small angle neutron scattering

The SANS data presented in this study was collected on the NG3 30 m SANS instrument (Glinka et al., 1998) at the National Institute of Standard and Technology Center for Neutron Research (NIST-CNR), Gaithersburg, MD, at the CG-3 Bio-SANS instrument (Heller et al., 2014) at the High Flux Isotope Reactor (HFIR) facility, Oak Ridge, TN, as well as on the D22 instrument (Laue-Langevin, 2019a) at the Institut Laue Langevin in Grenoble, France. Scattering intensity measurements taken over a broad Q-range: $0.001 \, \text{Å}^{-1} < Q < 0.6 \, \text{Å}^{-1}$ using a wavelength of 6 Å were used to characterize vesicles. Data is captured using a 2-D detector and reduced using the reduction packages provided by NIST-CNR (Kline, 2006) and ILL (Laue-Langevin, 2019b) yielding circularly averaged absolute intensity versus Q curves. In the case of kinetic measurements, the scattering intensity, $I(Q, t)$, was obtained using a single instrument configuration with a Q range between $0.003 \, \text{Å}^{-1} < Q < 0.04 \, \text{Å}^{-1}$ with data collection steps being as short as 30 s.

To render the lipid vesicles invisible for this study and only measure scattering from cholesterol, the *SLD* of the deuterated POPS and POPC vesicles were matched to that of the solvent by using a mixture of D_2O and H_2O. Using pure water rather than a buffer with serine lipids has been noted to not make a significant difference (Radhakrishnan and McConnell, 1999). The proper ratio of D_2O and H_2O was determined by measuring the SANS pattern from these POPS and POPC vesicles in varying mixtures of D_2O and H_2O. The contrast match point (point at which the *SLD* difference between the particles and the solvent equals zero) is obtained by plotting the square root of the background subtracted scattered intensity versus the volume fraction of D_2O (Garg et al., 2011). The match point for deuterated POPS was found to be at a volume fraction of 55.8% D_2O (Garg et al., 2014) while the match point for deuterated POPC we had previously found to be at 48.6% D_2O (Garg et al., 2011). All further experiments in this study were performed at the corresponding contrast match D_2O fraction congruent with either a POPS or a POPC membrane, which then rendered the lipids invisible to neutrons. Therefore all scattering was due to the presence of cholesterol in the vesicles.

4.3. Fluorescence spectroscopy

Fluorescence spectroscopy measurement for both Laurdan and DPH were done using a Horiba Fluoromax-4 spectrofluorometer. The emission spectra using Laurdan were obtained using an excitation wavelength of 340 nm. The generalized polarization function, *GP*, compares the relative emission intensities, after excitation, at 440 nm and 490 nm and given by (Jay and Hamilton, 2017):

$$\text{GP} = (I_{440} - I_{490})/(I_{440} + I_{490}) \tag{2}$$

where I_{440} and I_{490} are the corresponding relative intensities at 440 nm and 490 nm of normalized Laurdan emission spectra.

Anisotropy measurements from DPH were obtained from fluorescence emission intensity at 426 nm (363 nm excitation) and was measured with excitation and emission polarizers parallel to each other (both at 0°, I_0) and repeated with the polarizers perpendicular to each other (excitation: 0°, emission: 90°, I_{90}). Anisotropy was then calculated using the steady-state equation (Troup et al., 2006):

$$r = (I_0 - gI_{90})/(I_0 + 2gI_{90}) \tag{3}$$

The correction factor, *g*, is the ratio of emission intensity at 0° and 90° with the excitation polarizer oriented at 90°. The error bars correspond to five measurements per point.

References

Demchenko, A.P., Mely, Y., Duportail, G., Klymchenko, A.S., 2009. Biophys. J. 96, 3461.
Eeman, M., Deleu, M., 2010. Biotechnol. Agron. Soc. Environ. 14, 719.
Epand, R.M., Bain, A.D., Sayer, B.G., Bach, D., Wachtel, E., 2002. Biophys. J. 83, 2053.
Eyring, H., 1935. J. Chem. Phys. 3, 107.
Frazier, M.L., Wright, J.R., Pokorny, A., Almeida, P.F., 2007. Biophys. J. 92, 2422.
Garg, S., Porcar, L., Woodka, A.C., Butler, P.D., Perez-Salas, U., 2011. Biophys. J. 101, 370.
Garg, S., Porcar, L., Woodka, A.C., Butler, P.D., Perez-Salas, U., 2012. Biophys. J. 102, 947.
Garg, S., Castro-Roman, F., Porcar, L., Butler, P., Bautista, P.J., Krzyzanowski, N., Perez-Salas, U., 2014. Soft Matter 10, 9313.
Gerelli, Y., Porcar, L., Lombardi, L., Fragneto, G., 2013. Langmuir 29, 12762.
Glinka, C.J., Barker, J.G., Hammouda, B., Krueger, S., Moyer, J.J., Orts, W.J., 1998. J. Appl. Crystallogr. 31, 430.
Harris, F.M., Best, K.B., Bell, J.D., 2002. Biochim. Biophys. Acta 1565, 123.
Heller, W., Urban, V., Lynn, G., Weiss, K., O'Neill, H., Pingali, S., Qian, S., Littrell, K., Melnichenko, Y., Buchanan, M., Selby, D., Wignal, G., 2014. J. Appl Crystallogr. 47, 1238.
Homan, R., Pownall, H.J., 1988. Biochim. Biophys. Acta 938, 155.
Ikonen, E., 2008. Nat. Rev. Mol. Cell Biol. 9, 125.
Jay, A.G., Hamilton, J.A., 2017. J. Fluoresc. 27, 243.
Kleinfeld, A.M., Storch, J., 1993. Biochemistry 32, 2053.
Kline, S.R., 2006. J. Appl. Crystallogr. 39, 895.
Krzyzanowski, N., Porcar, L., Garg, S., Butler, P., Castro-Roman, F., Bautista, P.J., Perez-Salas, U., 2015. Soft Matter 11, 5582.
Kucerka, N., Marquardt, D., Harroun, T.A., Nieh, M.P., Wassall, S.R., de Jong, D.H., Schafer, L.V., Marrink, S.J., Katsaras, J., 2010. Biochemistry 49, 7485.
Laidler, M., Klng, K.J., 1983. J. Phys. Chem. 87, 2657.
Lakowicz, J.R., Prendergast, F.G., 1978. Biophys. J. 24, 213.
I. Laue-Langevin, 2019. D22, https://www.ill.eu/users/instruments/instruments-list/d22/description/instrument-layout/.
I. Laue-Langevin, 2019. Grasp, https://www.ill.eu/users/support-labs-infrastructure/software-scientific-tools/grasp/.
Lenz, B., 1989. Chem. Phys. Lipids 50, 171.
Leventis, R., Silvius, J.R., 2001. Biophys. J. 81, 2257.
Lingwood, D., Simons, K., 2010. Science 327, 46.
Masserini, M., Freire, E., 1987. Biochemistry 26, 237.
Maxfield, F.R., Tabas, I., 2005. Nature 438, 612.
Niu, S.L., Litman, B.J., 2002. Biophys. J. 83, 3408.
Parasassi, T., De Stasio, G., d'Ubaldo, A., Gratton, E., 1990. Biophys. J. 57, 1179.
Parasassi, T., De Stasio, G., Ravagnan, G., Rusch, R.M., Gratton, E., 1991. Biophys. J. 60, 179.
Radhakrishnan, A., McConnell, H.M., 1999. Biophys. J. 77, 1507.
Raguz, M., Mainali, L., Widomska, J., Subczynski, W.K., 2011. Biochim. Biophys. Acta 1808, 1072.
Simons, K., Ikonen, E., 1997. Nature 387, 569.
Simons, K., Vaz, W.L., 2004. Annu. Rev. Biophys. Biomol. Struct. 33, 269.
Soccio, R.E., Breslow, J.L., 2004. Arterioscler. Thromb. Vasc. Biol. 24, 1150.
Troup, G.M., Wrenn, S.P., Apel-Paz, M., Doncel, G.F., Vanderlick, T.K., 2006. Ind. Eng. Chem. Res. 45, 6939.
van Meer, G., Voelker, D.R., Feigenson, G.W., 2008. Nat. Rev. Mol. Cell Biol. 9, 112.
Wang, C., Yu, Y.M., Regen, S.L., 2017. Angew. Chem. Int. Ed. 56, 1639.